

The quark-gluon plasma: diagnosis with thermal hadron production from the early history until detailed characterization at high energy colliders

Peter Braun-Munzinger, Krzysztof Redlich, and Johanna Stachel

Abstract In nuclear collisions at relativistic energies, matter is created which resembles closely the matter that filled all space until about $15\ \mu\text{s}$ after the big bang. Here we summarize selected aspects of the research that led to the establishment of this new sub-field of physics and briefly describe its current ‘state of the art’ with emphasis on matter creation through thermal particle production. In particular, we will focus on particle production at low transverse momentum and explain how its analysis sheds light on one of the key open questions, i.e. what is the mechanism of hadronization of colored objects such as quarks and gluons.

1 Introduction and some historical context

The story actually starts long before QCD, the quantum field theory of the strong interaction, was developed. In the early 1950s it was realized that collisions between two protons in the GeV energy range led to multiple production of new particles (mostly pions). Their multiplicity exhibited features which could be understood in terms of a thermal approach [1–3]. With the advent of new higher energy accelerators at CERN (the CERN PS completed in 1959) and at Brookhaven (the BNL AGS completed in 1960) the stage was set to embark on a detailed study of how new particles are created in high energy proton-proton collisions. Very

Peter Braun-Munzinger

Extreme Matter Institute EMMI, GSI, 64291 Darmstadt, Germany and Physikalisches Institut, Universität Heidelberg, 69120 Heidelberg, Germany; e-mail: p.braun-munzinger@gsi.de

Krzysztof Redlich

Institute of Theoretical Physics, University of Wroclaw, 50204 Wroclaw, Poland and Polish Academy of Sciences PAN, 50449 Wroclaw, Poland; e-mail: krzysztof.redlich@uwr.edu.pl

Johanna Stachel

Physikalisches Institut, Universität Heidelberg, 69120 Heidelberg, Germany;
e-mail: stachel@physi.uni-heidelberg.de

soon it was realized that some aspects of the experimentally emerging collision dynamics exhibited features characteristic of thermal particle production [4–6]. Soon afterwards, other statistical approaches were published [7, 8].

In the early 1970s QCD was introduced with its novel features of infrared slavery and asymptotic freedom. These properties of QCD are outlined in detail in a recent review [9] and provide also the basis to describe strongly interacting matter in terms of thermodynamic phases. This was first realized by Collins [10]. Soon thereafter appeared the 1st phase diagram of QCD [11]. The term quark-gluon plasma (QGP) was actually coined soon afterwards by Shuryak [12] for the description of the high temperature phase where confinement gives way to de-confinement and chiral symmetry is restored. Similar arguments apply also for matter at high baryon density such as is found in the center of neutron stars.

This article is organized in the following way: we will first briefly summarize what is currently known about the QGP from first principle QCD. This is obtained by solving the QCD equations by introducing a discrete space-time lattice, i.e. using lattice QCD (lQCD). After a brief review of global quantities characterizing the QGP, the hadron resonance gas (HRG) is introduced. A good recent introduction into the physics behind the HRG is given in [13].

The key idea behind the HRG approach originates from the work of [4] and is the following: to derive thermal properties of a system of strongly interacting particles (hadrons or quarks and gluons) in equilibrium one needs the statistical partition function. In QCD this is directly obtained from the basic constituents (quarks and gluons) and their interaction encoded in the QCD Lagrangian. Since no analytic solution of the QCD equations is available to date a promising alternative approach is to build the partition function from all known hadrons. Implicitly one can argue that, for temperatures not too far from the QCD phase transition temperature, the complete spectrum of hadrons already comprises all of QCD. Also, for such relatively low temperatures, a next step is then to neglect all interactions among hadrons. If one knows the masses and quantum numbers of all hadrons along with their strong decay probabilities it is then fairly straightforward to build the complete partition function. From this partition function one can compute all needed thermodynamic quantities such as energy density, entropy density and particle density. Explicit details are given in [13–15].

An important refinement is to take (residual) interactions in the HRG description via the S-matrix approach. This is briefly introduced in the section on S-matrix thermodynamics below. Another important development is the introduction of conserved quantum numbers into the thermal approach. This leads directly to thermodynamical concepts for the QGP and forms the basis of the statistical hadronization model (SHM) when coupled to a prescription on how hadrons are formed at the QCD phase boundary. This prescription essentially follows the ideas developed in [16].

We will dominantly focus on the global properties of integrated yields of particles produced in hadron and heavy ion collisions. This will allow us to address the concept of their thermal origin and to identify the equation of state of the fireball produced in the collision. This is particularly transparent at the highest collision energies at

the LHC, where measured yields of light-quark hadrons are shown to be consistent with the lQCD equation of state at the QCD phase boundary.

Identification of the thermal origin of hadron production is therefore the prerequisite before proceeding to the study of interesting collective and dynamical phenomena outside the scope of the SHM. Also the majority of studies of fluctuations and correlations as well as investigations of critical properties linked to the chiral phase transition occurring in hot and dense QCD matter [17] are performed within the framework of statistical theories [18, 19].

A high degree of thermal equilibrium is equally necessary to analyze the expansion dynamics of the fireball [20], and its transverse and elliptic flow [21, 22] with the tools of relativistic hydrodynamics. Investigations into the microscopic origin of parton energy-loss [23] and experimental and theoretical studies of electromagnetic emissivity in heavy-ion collisions have brought interesting insights into properties of the QGP medium [24, 25].

Many of these interesting aspects are outside of the scope of the present article and are therefore only mentioned and cited here. We do discuss below in some detail the case of multi-charm hadrons and their special role in the QGP as it is presently our only means to shed light on the crucial question of the degree of deconfinement of the medium under investigation [9, 15].

We demonstrate the predictive power of the SHM for the description of experimental particle yields for hadrons composed of light (u,d,s) valence quarks. For an extension of SHM to heavier quarks we introduce the concept of the heavy quark (charm or beauty) balance equation and demonstrate that this leads to a parameter-free extension to the charm sector (SHMc) as demonstrated by comparing to relevant experimental data. We follow with a short section on the possible role of charm quarks in the QGP equation of state and end with a brief summary.

2 Short summary of recent results from lQCD

In the thermodynamic limit, i.e under the assumption of thermal equilibrium, the full QCD partition function, and hence the equation of state, can be computed without further assumptions, although limits from computer technology initially did not allow inclusion of dynamical quarks. The first lQCD calculations of the equation of state were performed in the early 1980s [26]. Already then a close link emerged between deconfinement and restoration of chiral symmetry [27]. With increasing computing power the following four decades brought a real breakthrough in finite temperature lQCD.

Recent numerical lQCD calculations [28] show, for massless u and d quarks and at vanishing chemical potential, evidence for a true second-order chiral transition between hadron gas and QGP at a critical temperature of $T_c \approx 132^{+3}_{-6}$ MeV. For realistic u,d,s-quark masses, the chiral transition is rather a crossover at a precisely determined pseudo-critical temperature of $T_{pc} = 156.5 \pm 1.5$ MeV [29]. Independent

confirmation came from [30], where a transition temperature of 158.0 ± 0.6 MeV was reported. For a very recent review, see [31].

Extending the lQCD calculations into regions of finite net baryon density quantified by a baryon chemical potential μ_B [29, 30] is now possible by expansion techniques. Current lQCD expansion techniques already cover the regime of $\mu_B/T \leq 3$. The so obtained phase transition line of pseudo-critical temperatures is shown in the QCD phase diagram displayed in Fig 2 below. The sign problem so far prevents use of this technique in regions of larger values of μ_B , see e.g. [32]. There one has to resort to models of QCD for further exploration. All indications point since a long time to a very similar temperatures and phase transition line for the deconfinement transition.

3 Brief summary of experimental results on global QGP properties

Experimentally, this regime of the QCD phase transitions is accessible by investigating collisions of heavy nuclei at high energy. It was conjectured already in [8] that, in such hadronic collisions, after some time local thermal equilibrium is established and all properties of the system (fireball) are determined by a single parameter, the temperature T , depending on time and spatial coordinates. This is exactly the regime probed by collisions of nuclei at the Large Hadron Collider (LHC), as will be outlined in the following. The region of finite to large μ_B is accessed by nuclear collisions at lower energies.

In the early phase of the collision, the incoming nuclei lose a large fraction of their energy leading to the creation of a hot fireball characterized by an energy density ϵ and a temperature T . The concomitant deceleration of the nucleons in the colliding nuclei, called stopping, is characterized by an average rapidity shift $\Delta y = -\ln(E/E_0)$ with nucleon energies E and E_0 before and after the collision. Quantitative information is contained in the experimentally measured net-proton rapidity distributions (i.e. the difference between proton and anti-proton rapidity distributions). These distributions are summarized for collision energies from the SPS to RHIC energy range in [33]. Including also the AGS data it emerges that the rapidity shift saturates at approximately two units from $\sqrt{s_{NN}} \approx 17.3$ GeV upwards, implying a fractional energy loss of $1 - \exp(-\Delta y) \approx 86\%$. In fact, the same rapidity shift was already determined for p–nucleus collisions at Fermilab for 200 GeV/c proton momentum [34] compared to about one unit for pp collisions. With increasing collision energy, the target and projectile rapidity ranges are well separated, leaving at central rapidity with a small or even zero net-baryon density, and universal fragmentation regions forward and backward following the concept of limiting fragmentation [35].

The energy loss (rapidity shift) of the incident nucleons leads to high energy densities at central rapidity, i.e., in the center of the fireball. These initial energy densities can be estimated using the Bjorken model [36]:

$$\epsilon_{BJ} = \frac{1}{A\tau_0} \frac{dE_T}{d\eta} \frac{d\eta}{dy}, \quad (1)$$

where $A = \pi r^2$ is the overlap area of two nuclei and the kinetic equilibration time τ_0 . Eq. 1 is typically evaluated at a time $\tau_0 = 1$ fm and the resulting energy densities are displayed in Table 1 for central Au–Au and Pb–Pb collisions at the different collision energies. For central Pb–Pb collisions ($A = 150$ fm 2) at $\sqrt{s_{NN}} = 2.76$ TeV this yields an energy density of about 14 GeV/fm 3 [37], more than a factor of 30 above the critical energy density for the chiral phase transition as determined in lQCD calculations. In fact, for all collision energies shown the initial energy density significantly exceeds that computed in lQCD at the pseudo-critical temperature, indicating that the matter in the fireball is to be described with colored quark and gluon degrees of freedom rather than as hadronic matter. The corresponding initial temperatures can be computed using the energy density of a gas of quarks and gluons with two quark flavors, $\epsilon = 37 \frac{\pi^2}{30} T^4$, yielding e.g. $T \approx 307$ MeV for LHC energy. Temperature values for lower collision energies are also quoted in the Table¹.

	$\sqrt{s_{NN}}$ [GeV]	$dE_t/d\eta$ [GeV]	ϵ_{BJ} [GeV/fm 3]	T [GeV]
AGS	4.8	200	1.9	0.180
SPS	17.2	400	3.5	0.212
RHIC	200	600	5.5	0.239
LHC	2760	2000	14.5	0.307

Table 1 Collision energy per colliding nucleon pair, measured transverse energy pseudo-rapidity density at mid-rapidity [37–40], energy density, and initial temperature estimated as described in the text for central Pb–Pb and Au–Au collisions at different accelerators.

Depending on energy, collisions of heavy ions populate different regimes falling into two categories: (i) the stopping or high baryon density region reached at $\sqrt{s_{NN}} \approx 3\text{--}20$ GeV and (ii) the transparency or baryon-free region reached at higher collision energies. The net-baryon-free QGP presumably existed in the early universe after the electro-weak phase transition and up to about 15 microseconds after the Big Bang. This corresponds to the time of the QCD phase transition, where the strongly interacting constituents, i.e. the quarks and gluons, are converted into hadrons. For a brief but concise description, see section 22.3 of [41]. In the QGP of the early universe, particles interacting via the strong and electro-weak force are part of the system, while an accelerator-made QGP only contains strongly interacting particles.

¹ The values reported in the table are all for vanishing chemical potentials. We have evaluated the differences if one assumes values for chemical potentials as determined at chemical freeze-out, see below. The resulting temperature values differ by less than 5% from those reported in Table 1. Owing to the proportionality of energy density to the fourth power of temperature, inclusion of a bag pressure only mildly changes the calculated temperature values.

On the other hand, a baryon-rich QGP may be produced in neutron star mergers or could exist, at very low temperatures, in the center of neutron stars [42–44].

Another important difference between the ‘laboratory-created’ QGP and the QGP phase in the early universe is that, after the QCD phase transition, the ‘laboratory-created’ QGP falls out of equilibrium and never returns. This is denoted as chemical freeze-out. In contradistinction, the standard model phase, which now contains hadrons, leptons, photons and neutrinos, immediately returns to equilibrium and stays there until neutrino-freeze-out at a time of about 1 s after the big bang. For a detailed description of this phase see [45].

4 S-matrix thermodynamics of strong interactions

A fireball produced in particle or nuclear collisions can be described as a thermal medium composed of hadrons as leading constituents. The thermodynamics of such a system is described in terms of an interacting gas of ground-state hadrons. The S-matrix formalism is a theoretical framework to implement interactions in a dilute many-body hadronic system in thermal and chemical equilibrium [46–50]. There, the thermodynamic pressure for a hadronic gas at finite temperature and density, formulated in the Grand-Canonical (GC) ensemble, undergoing two-body scatterings, $h_1 + h_2 \rightarrow h_1 + h_2$, is expressed as

$$P(T, \mu) = \sum_i P_i^{id} + \Delta P^{int}, \quad (2)$$

where P_i^{id} corresponds to an ideal gas contribution of hadron h_i . The interaction part of the thermodynamic pressure due to two-body scatterings ΔP^{int} involves an integral over the invariant mass M [48],

$$\Delta P_{int.} \approx \sum_{I,j} \int_{m_{th}}^{\infty} dM \frac{1}{\pi} \frac{d\delta_j^I}{dM} P_i^{id}(M) \quad (3)$$

where δ_j^I is the scattering phase shift for a given isospin-spin channel.

The pressure of a non-interacting gas of particles and their anti-particles carrying mass m_i and spin-isospin degeneracy factor d_i , under Boltzmann statistics, reads²

$$P_i^{id} = \frac{d_i}{2\pi^2} m_i^2 T^2 \left(\lambda_i + \frac{1}{\lambda_i} \right) K_2 \left(\frac{m_i}{T} \right), \quad (4)$$

where $\lambda_i = \exp[(B_i \mu_B + S_i \mu_S + Q_i \mu_Q)/T]$ is the fugacity, and $\mu = (\mu_B, \mu_S, \mu_Q)$ is the chemical potential linked to the GC implementation of charge-conservation laws

² We use the Boltzmann distribution for simplicity. The extension to quantum statistics can be found in Refs. [14, 49] and is applied when doing quantitative investigations.

with B_i, S_i, Q_i being the baryon number, strangeness and electric charge of particle, i , respectively.

In the presence of attractive interactions driven by a resonance of mass m and vanishing width, $\Gamma \simeq 0$, the effective density of states approaches a delta function,

$$\frac{1}{\pi} \frac{d\delta_j^I}{dM} \rightarrow \delta(M - m). \quad (5)$$

Consequently, the interaction part of the pressure acts as an ideal gas of resonances. For a finite resonance width, the spectral density is linked to the standard Breit-Wigner distribution,

$$\frac{d}{dM} \delta_{\text{res}}(M) \rightarrow B(M) = \frac{2M^2\Gamma}{(M^2 - m^2)^2 + M^2\Gamma^2}. \quad (6)$$

In the limit $\Gamma \rightarrow 0$ the spectral density converges to Eq. 5.

Thus, in leading order in the density expansion, accounting only for attractive interactions driven by resonance formation, the thermodynamic pressure of strongly interacting hadron gas can be approximated as a mixture of ideal gases of all stable hadrons, resonances, and their antiparticles,

$$P^{\text{HRG}}(T, \mu) = \sum_i P_i^{\text{id}} + \sum_k P_k^{\text{res}}. \quad (7)$$

The first sum runs over all stable hadrons, whereas the second term quantifies the contribution of all known resonance states, where

$$P_k^{\text{res}} = \int_{m_{th}}^{\infty} \frac{dM}{\pi} B(M) P_k^{\text{id}}. \quad (8)$$

This approximation of the S-matrix constitutes the well-known Hadron Resonance Gas (HRG) model [14, 15].

4.1 Hagedorn's limiting temperature

The HRG thermodynamic potential in Eq.7 is a discrete representation of the statistical-thermodynamical approach to strong interactions at high energies formulated by Rolf Hagedorn in 1965, based on the concept of the statistical bootstrap [4, 51] (see also [52] and references therein). He assumed that, at high collision energies, higher and higher resonances (fireballs) of strongly interacting hadrons are formed and take part in the thermodynamics as if they were stable particles. A self-similar scheme for the composition and decay of resonances led Hagedorn to the solution of their exponential mass spectrum,

$$\rho(m) = \text{const} \cdot m^a \exp(m/T_H), \quad (9)$$

where $a = -5/2$ [4]. Consequently, the pressure of resonances corresponding to the above $\rho(m)$ becomes [51]

$$P_H(T) \simeq \frac{T^2}{2\pi^2} \int_{m_0}^{\infty} dm m^2 \rho(m) K_2\left(\frac{m}{T}\right) \quad (10)$$

The exponential form of $\rho(m)$ implies that T_H becomes the upper limit of permissible temperature of hadronic matter. See also the discussion about this in [53]. The power law coefficient a determines the behavior of different thermodynamic quantities at $T \simeq T_H$. With the value of $a = -5/2$ obtained by Hagedorn, the pressure, energy density and the specific heat diverge at T_H . This is what made Hagedorn conclude that T_H , known today as Hagedorn's temperature, is indeed the highest possible temperature of hadronic matter. On the other hand, for a lower value of a , in particular, for $a = -7/2$ as expected e.g. from the Veneziano model [54], the energy density remains finite at T_H , shifting the divergence to the specific heat [55]. Also, formulating Hagedorn's model for extended particles can provide a finite energy density at T_H for larger values of a [56]. Such a behavior of thermodynamic quantities is usually linked to the transition to a new phase of matter. Today, one connects this to the transition from hadronic matter to a quark-gluon plasma. Furthermore, the value of the Hagedorn temperature, extracted from different implementations of the bootstrap conditions [51, 52], or from the recent fit of $\rho(m)$ to data [57–59], lies in the range $135 < T_H < 190$ MeV. This range contains the precisely determined chiral crossover temperature $T_c \simeq 156.5$ MeV, calculated within the framework of lQCD (see above).

4.2 Linking the HRG with the QCD thermodynamics of the hadronic phase

A long-lasting question was whether the HRG model approximation of the thermodynamic potential of the hadronic phase that accounts for only attractive interactions is consistent with QCD thermodynamics. The answer and justification were given by directly comparing the equation of state obtained in lQCD and from the HRG [60–67], see also [68] or Hagedorn's model [57, 69]. It turned out that the temperature dependence of pressure, energy density and entropy density is well described by the HRG equation of state up to the near vicinity of the chiral crossover. Such an agreement is direct evidence that the thermodynamic potential of the HRG already provides a good approximation to QCD thermodynamics of the confined phase. Interestingly, by comparing HRG model results with lQCD results, it was shown that there must be missing resonances beyond those listed in the PDG [41], particularly in the strange-baryon and charmed-baryon sectors [69–71].

4.3 Statistical Hadronization Model and hadron production yields

From the partition function of HRG it is rather straightforward to calculate the particle composition of a fireball of volume V and with thermal parameters (T, μ) [14, 15, 72]. The total multiplicity $\langle N_i \rangle$ of particle i is obtained, as

$$\langle N_i \rangle = \langle N_i \rangle^T + \sum_r B(r \rightarrow i) \langle N_r \rangle^{res}. \quad (11)$$

The first term is the thermal average number of particles i . The second term describes the overall contribution from resonances decaying to i . The $B(r \rightarrow i)$ is the corresponding decay branching of resonance r to final state hadron i . In the Boltzmann approximation, enter the thermal yields of stable particles, $\langle N_i \rangle^T = (V/T) P_i^{id}$ with P_i^{id} from Eq. 2, and of resonances $\langle N_r \rangle^{res} = (V/T) P_r^{res}$ with P_r^{res} as in Eq. 8.

The numerical implementation of Eqs. (7-11), extended to quantum statistics, constitute the Statistical Hadronization Model (SHM), as given in [15] and refs. there. This model has been successfully applied to quantify thermalization and particle production yields in hadron and heavy ion collisions (see the discussion below).

We note, however, that some of the simplifying assumptions as e.g. that of attractive interactions implicit in the above HRG model are not necessarily consistent with hadron scattering data. In particular, for an accurate implementation of interaction effects, a proper resonance invariant mass distribution, the presence of non-resonant contributions, as well as repulsive interactions, have to be included to be consistent with scattering data. This can be done systematically within the S-matrix approach where two-body interactions are included via the empirical scattering phase shifts as in Eq. 3. The resulting interacting density of states is then folded into an integral over thermodynamic distribution functions which, in turn, yields the contribution from interactions to a particular thermodynamic quantity.

The phenomenological implications and importance of the S-matrix approach have been recently quantified in the context of particle production in heavy ion collisions, and in the description of lQCD results on different fluctuation and correlation observables of conserved charges in the hadronic phase. In particular, it was demonstrated that the implementation of the empirical pion-nucleon phase shifts is crucial for the quantitative description of lqcd results on the baryon-charge susceptibility [49]. Also in the analysis of proton production yields in nucleus-nucleus collisions at the LHC, a careful treatment of empirical pion-nucleon scattering phase-shifts could resolve the proton-yield anomaly [73]. Furthermore, in the strange baryon sector of the HRG, the improvement of interactions within the S-matrix formalism was shown to increase the strange-baryon correlations towards lQCD results up to $T \simeq T_c$ [74, 75].

4.4 Exact charge conservation

The HRG model for particle production introduced in Eq. 7 is formulated in the Grand Canonical (GC) ensemble concerning charge conservation laws. The conservation of baryon number, strangeness, and electric charge holds on average and is controlled by the corresponding chemical potentials. It is already well established, however, that such a GC model can only be applied if the number of produced charged particles is sufficiently large. If this is not the case, a thermal description requires exact implementation of charge conservation, as introduced in the canonical C-ensemble [14, 51, 76–81]. This is particularly the case when applying the thermal model to particle production in pp and pA collisions, as well as in low-energy heavy-ion collisions and even at the LHC when considering events with low charged-particle multiplicity. In general, in collisions the conservation of quantum numbers is fulfilled exactly as the initial conditions fix them.

The yields of charged particles calculated in the C-ensemble are usually suppressed relative to the values obtained in the GC-ensemble [14, 77, 79, 82]. The HRG model formulated in the C-ensemble has provided an instrumental framework for the centrality and system-size dependence of particle production and in particular strangeness production and suppression [79, 80, 83]. The applicability of the model in small systems like pp [84, 85], pA [86] and e^+e^- collisions has been successfully verified in the literature [87, 88].

In particular, the characteristic prediction of the HRG model in the C-ensemble was an increasing suppression of strange particle yields per pion with decreasing collision energy and collision centrality, as well as with increasing strangeness content of the particle [80, 83]. Such a pattern of suppression of (multi-)strange hadrons with decreasing multiplicity was indeed observed by the ALICE collaboration [89] and is qualitatively similar to what has been measured previously by the WA97 and NA57 collaborations at SPS energies at CERN [90] and by the STAR collaboration at RHIC [91]. The recent ALICE data on (multi)strange particle production, as well as data on kaon excitation functions at lower energies, are consistent with predictions of the thermal model accounting for exact strangeness conservation formulated in the canonical ensemble [92–94].

5 Hadron production at the QCD phase boundary: a contemporary view

5.1 Integrated yields (u,d,s) hadrons

Experimental information on the equation of state of QCD matter near the phase boundary, and hence on the QCD phase diagram, is obtained from the measurement of the yields of hadrons produced in (central) high energy nuclear collisions. Analysis of data in the framework of the SHM makes use of Eq. 11, see [15] and refs. there,

since there it is demonstrated that at hadronization, when the colored quarks and gluons are transformed into colorless hadrons, the fireball formed in the collision is very close to a thermodynamic state in full (hadro-)chemical equilibrium.

From Eq. 11 one obtains directly the first moments (mean values) of the densities of hadrons as a function of a pair of thermodynamic parameters, the temperature T_{chem} and the baryon chemical potential μ_B at chemical freeze-out. Note that after chemical freeze-out, the fireball is rapidly falling out of equilibrium. Expansion and cooling will move it further away from equilibrium [95]. This situation is very different from the evolution in the early universe where the cooling rate is very slow compared to typical hadronic interaction times of order 10^{-23} s and the system continuously adjusts to thermal equilibrium for an extended period.

To go beyond the non-interacting HRG gas approximation, attractive and repulsive interactions between hadrons can be taken into account in the S-matrix formulation of statistical mechanics, as discussed above. The predictions of the SHM for hadron yields, including the S-matrix correction for protons, are compared to experimental data at LHC energy for $T_{\text{chem}} = 156.5$ MeV in Fig. 1. The agreement between model predictions and data is excellent for all measured hadron species, including nuclei and hyper-nuclei. Since the value of the baryo-chemical potential turns out to be consistent with zero, all anti-particle yields agree with those of the corresponding particles, with yields varying over 9 orders of magnitude. Remarkably, the description works also for loosely bound states, i.e. atomic nuclei where the nucleon separation energy is much smaller than the temperature of the system.

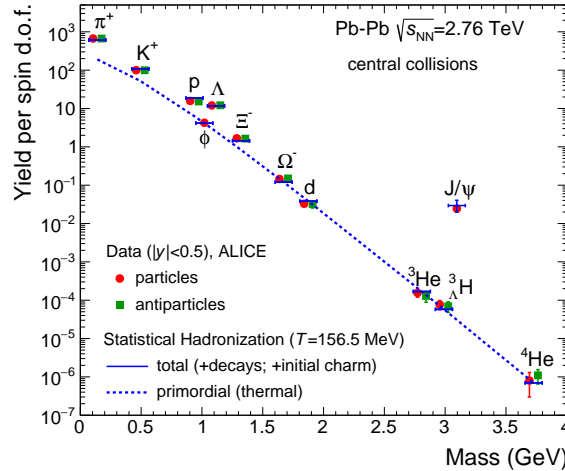


Fig. 1 Experimental rapidity densities normalized to the spin degeneracy for LHC data compared to primordial and total (anti-)particle yields as calculated within the SHM [15].

The values of the hadro-chemical freeze-out parameters determined through measurements at lower collisions energies are likewise obtained by fitting the SHM predictions to the measured hadron yields. The so extracted freeze-out parameters

T_{chem} and μ_B [15, 96, 97] are presented as red symbols in the QCD phase diagram shown in Fig. 2. The experimental freeze-out points are compared to the crossover chiral phase transition line as computed in lQCD (shown as the blue band). For all center-of mass energies from LHC energies on down to about $\sqrt{s_{\text{NN}}} = 12$ GeV, i.e., over the entire range covered by lQCD, there is a remarkably close agreement visible between T_{chem} and the pseudo-critical temperature for the chiral cross over transition T_{pc} . We note that, along this phase boundary, the energy density computed (for 2 quark flavors) from the values of T_{chem} and μ_B exhibits a nearly constant value of $\epsilon_{\text{crit}} \approx 0.46$ GeV/fm³.

The experimental result that the chemical freeze-out temperature turns out to be close to T_{pc} has a fundamental reason: because of the very rapid temperature and density change across the phase transition and afterwards due to the rapid expansion, the resulting low hadron densities in the fireball combined with its size cause inelastic interaction between hadrons to cease within a narrow temperature interval of a few MeV [95] after hadron formation.

As already indicated above, this rapid chemical freeze-out is actually very different from the continuous slow decoupling taking place in the early universe. To emphasize the different time and distance scales relevant there, we note that for temperatures T larger than a few MeV even the mean free path for neutrinos is much smaller than the size of the universe, see section 22.3 of [41]. The slow decoupling after the QCD phase transition implies baryon-antibaryon annihilation and, due to the very small initial baryon-antibaryon asymmetry, to an increasing baryon chemical potential. The trajectory of the early universe in the QCD phase diagram thereby takes a somewhat unexpected course [98]. See also the discussion at the end of section 3 above. Due to this baryon asymmetry (still not understood, for a discussion see section 22.3.6 in [99]), annihilation in the early universe stops when all antibaryons are ‘consumed’. The surviving protons and neutrons form nuclei, in competition with neutron decay, when the temperature has reached the MeV scale. The final outcome of this is described well in Steven Weinberg’s textbook ‘The First Three Minutes’ [100].

For values of baryon chemical potential beyond 400 MeV, implying higher baryon density beyond the current reach of lQCD, experimental data for chemical freeze-out have also been measured but the resulting phase structure of strongly interacting matter at high baryon density is still not well understood. Calculations based on various model approaches imply the appearance of a line of first order phase transition. Combined with the crossover transition at smaller values of the baryon chemical potential this would imply the existence of a critical end point (CEP) in the QCD phase diagram as indicated in Fig. 2. The experimental discovery of the CEP would mark a major break-through in our understanding of the QCD phase structure. If it exists, the location of the CEP is most likely in the region $\mu_B > 500$ MeV based on functional methods applied to QCD [101] and extrapolations from lQCD. Searching for the CEP is the subject of a very active research program, at RHIC and the future FAIR facility at GSI [102].

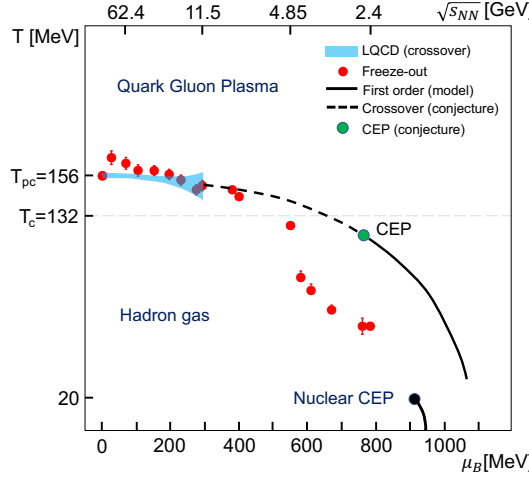


Fig. 2 Phase diagram of strongly interacting matter. The red symbols correspond to chemical-freezeout parameters, temperature T_{chem} and baryon chemical potential μ_B determined from experimental hadron yields [15, 96, 97]. The blue band represents the results of lQCD computations of the chiral phase boundary [29, 30]. Also shown are a conjectured line of first order phase transition with a critical end point as well as the nuclear liquid-gas phase boundary. This figure is from [9].

5.2 Extension to the heavy quark sector

With the impressive progress in particle identification of the four large LHC experiments significant new information is obtained on particle production in relativistic nuclear collisions. In particular, there is much progress for hadrons with open and hidden charm and beauty. In addition, there is mounting evidence [103–105], that hadrons composed of charm quarks reach a large degree of thermal equilibrium, although charm quarks in the system initially are chemically far out of equilibrium. This is supported by heavy quark diffusion coefficients from lQCD [106]. A strong indication for equilibration is the fact that J/ψ mesons participate in the collective, anisotropic hydrodynamic expansion [107, 108].

To microscopically understand the production mechanism of charmed hadrons for systems ranging from pp to Pb–Pb, various forms of quark coalescence models have been developed [109–113]. This provides one way to study the dependence of production yields on hadron size and, hence, may help to settle the still open question whether the many exotic hadrons that have been observed recently are compact multi-quark states or hadronic molecules (see [114, 115] and refs. cited there). Conceptual difficulties with this approach are that energy is not conserved in the coalescence process and that color neutralization at hadronization requires additional assumptions about quark correlations in the QGP [116].

Our own approach, named SHMc, has been made possible by the extension of the SHM to also incorporate charm quarks. This essentially parameter-free was

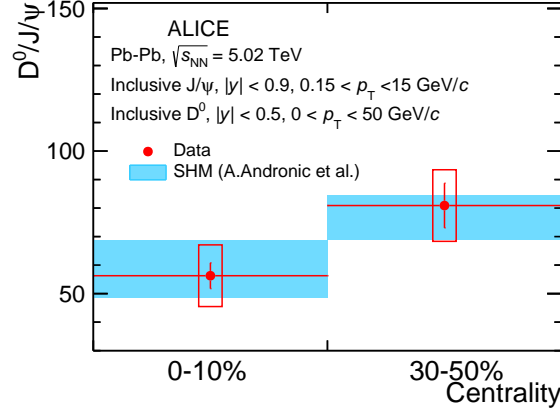


Fig. 3 D^0 to J/ψ yield ratio measured in $Pb-Pb$ collisions at the LHC and predicted by the Statistical Hadronization Model with charm SHMc. Figure from [117].

first proposed in [118] and developed further in [15, 119–123]. A comprehensive discussion is given in [104] and includes in SHMc all presently known hadrons with hidden and open charm. Importantly, the role of charmonia is not special anymore: they are treated as all other charmed hadrons. The key idea behind this is the recognition that, contrary to what happens in the (u,d,s) sector, the heavy (mass ~ 1.2 GeV) charm quarks are not thermally produced. Rather, production takes place in initial hard collisions. The produced charm quarks then thermalize in the hot fireball, but the total number of charm quarks is conserved during the evolution of the fireball [122] since charm quark annihilation is very small.

In essence, in this special thermal approach charm quarks can be treated like impurities in the hot fireball. Their description then requires the introduction of a charm fugacity g_c [104, 118]. The value of g_c is not a free parameter but experimentally determined by measurement of the total charm cross section. For central $Pb-Pb$ collisions at LHC energy, $g_c \approx 30$ [104]. An important consequence of the large fugacity is a strong increase in charmed hadron production compared to predictions from a purely thermal approach where $g_c = 1$. The charmed hadrons are, in the SHMc, all formed at the phase boundary, i.e. at hadronization, in the same way as all (u,d,s) hadrons.

In Fig. 1 it can be seen that, with that choice, the measured yield for J/ψ mesons is very well reproduced, the uncertainty in the prediction is mainly caused by the uncertainty in the total charm cross section in $Pb-Pb$ collisions. The enhancement visible for the J/ψ meson compared to the purely thermal prediction equal a factor g_c^2 then, since the J/ψ contains two charm quarks. We note here that, because of the formation from deconfined charm quarks at the phase boundary, charmonia are unbound inside the QGP but their final yield exhibits enhancement compared to expectations using collision scaling from pp collisions, contrary to the original predictions based on [124]. For a detailed discussion see [15].

For the description of yields of charmonia, feeding from excited charmonia is very small because of their strong Boltzmann suppression. For open charm mesons and baryons, this is not the case and feeding from excited D^* and Λ_c^* hadrons is an essential ingredient for the description of open charm hadrons [104, 123]. Even though the experimental delineation of the mass spectrum of excited open charm mesons and baryons is currently far from complete, the prediction of yields for D-mesons and Λ_c baryons compares very well with the measurements³, both concerning transverse momentum and centrality dependence.

The successful prediction of yields of hadrons with more than 1 charm quark is also direct evidence that charm quarks are deconfined inside the fireball formed in nuclear collisions at LHC energy. The typical size of this deconfined system has linear dimension of order 10 fm. The apparent absence of string-like forces with typical range of about 1 fm inside this hot system is fully consistent with the presence of deconfined charm quarks and indicates that also all light quarks could be deconfined. The topic of deconfinement in high energy nuclear collisions is also discussed in [9, 15].

A quite spectacular hierarchy of enhancements then emerges if one compares the predicted yields of single, double and triple charm hadrons. This is exhibited in Fig. 4.

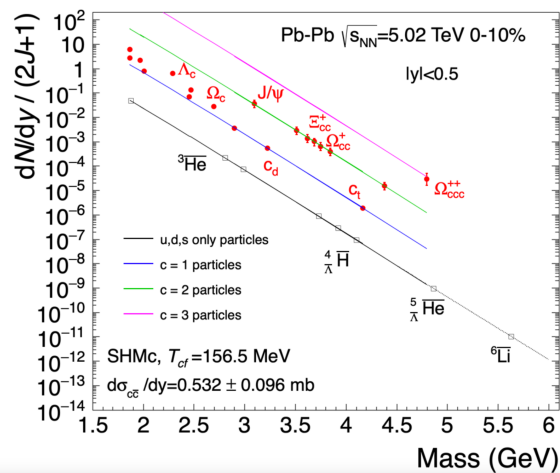


Fig. 4 Predictions of yields for singly- and multiply-charmed hadrons by the Statistical Hadronization Model with charm SHMc. Figure from [104] and adapted to include also selected light nuclei and hyper-nuclei.

Future measurement campaigns at the LHC in Run 3 and Run 4 and with ALICE [125] will yield detailed information on the production cross sections of hadrons

³ For Λ_c baryons one has to augment the currently measured charm baryon spectrum with additional states to achieve complete agreement with experimental data [104, 123].

with multiple charm quarks as well as excited charmonia. We expect that experimental tests of these predictions will lead to a more fundamental understanding of confinement/deconfinement and hadronization. Note that hadrons with two or more charm quarks cannot be produced in a single nucleon-nucleon collision. Confirmation of the SHMc prediction for multi-charm hadrons would imply that also the hadronization of these exotic hadrons can be described with a single parameter, i.e. the (pseudo-)critical temperature of the QCD cross-over phase transition.

An instructive way to proceed is obtained by analyzing the centrality dependence of the yield ratio $D^0/(J/\psi)$ for Pb–Pb collisions and comparing the results to the predictions of the SHMc. These D^0 and J/ψ production cross sections have for the 1st time been measured down to $p_t = 0$. The experimental yield ratio $D^0/(J/\psi)$ is in very good agreement with the SHMc prediction, as demonstrated in Fig. 3. This result buttresses the interpretation that open and hidden charm states are both produced by statistical hadronization at the phase boundary. An informative comparison between SHMc predictions and data for a number of open charm hadrons is shown in [104].

For center-of-mass energies $\sqrt{s_{NN}} \geq 10$ GeV the chemical freeze-out parameters closely agree with the phase boundary line obtained from lQCD [29, 30]. We conclude that hadronization from a equilibrated fireball is independent of particle species and only dependent on the values of T and μ_B at the phase boundary. At LHC energies where the chemical potential vanishes with good precision [126], only the freeze-out temperature $T = T_{pc}$ is needed to describe hadronization.

6 Short remarks on charm quarks and the QGP equation of state

The role of charm degrees of freedom on the hot matter equation of state has recently been investigated using the tools of lQCD [127, 128]. Since charm quarks are heavy, with a mass near 1.27 GeV (at a scale of 2 GeV [41]) they are very rare. In a hot fireball at temperature $T = T_{pc}$, and in full grand-canonical equilibrium, as is assumed in lQCD calculations, the number of charm quarks in a fireball with volume of 4000 fm³ per unit rapidity is 0.03, rising to 3.3 at $T = 2T_{pc}$. At that level, the charm quarks make negligible contributions to the energy density, and hence, equation of state of the QGP. However, in high energy nuclear collisions, the large majority of charm quarks in the fireball is not created thermally, but in initial hard collisions [15, 118] and subsequently thermalized in the hot QGP. For a central Pb–Pb collisions at $\sqrt{s_{NN}} = 5.02$ TeV this translates into about 13 charm quark pairs per unit rapidity [104]. This implies that about 3.5 % of the critical energy density is contained in charm quarks, not large, but maybe not negligible anymore. Whether the ‘quenched dynamical quarks’ approximation underlying the work of [127] is applicable here is also an open question. For conditions expected for the Future Circular Collider FCC there will be further increased initial charm production and likely substantial thermal charm production [129, 130] which could lead to large (of order 20 - 30 %) contributions by charm quarks to the QGP energy density and imply significant changes in the QGP equation of state. It would be very

interesting to add the appropriate ‘non-thermal’ number of charm quarks into 1QCD calculations to test this.

7 Summary

The pioneering papers [1–3] of the 1950s provided the basis for the first phenomenological investigations of early data on hadron production in high energy pp collisions [4] based on thermodynamical concepts. Since these very early days many experimental and theoretical/phenomenological analyses and publications have demonstrated the importance and usefulness of the statistical hadronization models which emerged over the course of the past 50 years. For a rather concise summary of the literature see [15]. We note here in particular two examples of the use of SHM and SHMc to provide insight into the physics of the QGP. In the year 2006 two papers appeared nearly simultaneously (but based on separate investigations) on the energy dependence of thermodynamic parameters [131, 132]. These papers together have to-date (May 2025) more than 1700 citations and provide the basis for many quantitative QGP studies. In the year 2021 a paper appeared on multi-charm hadron production and the mechanism of hadronization. This paper has laid the basis for part of the physics program of the new ALICE 3 [125] experiment at the ‘High Luminosity LHC’.

Of course there are also physics results which cannot be directly obtained from the SHM or SHMc. To compute, in addition to particle multiplicities, also the corresponding transverse momentum distributions or particle flow coefficients one needs to connect SHM with dynamical models. This has recently been achieved [133] by coupling the SHM(c) to models based on relativistic hydrodynamics, with good success. However, the thermal approach underlying SHM clearly breaks down for systems far off thermal equilibrium. Particle production at high transverse momentum, such as jet production, or processes involving energy loss of quarks and gluons in the dense fireball formed in high energy nuclear collisions cannot be described in the thermal framework outlined here. Surprisingly, the thermal approach works well to understand the particle multiplicities within a given jet, even for jets originating from e^+e^- collisions [87, 88, 134].

8 Acknowledgments

We acknowledge continued and long-term collaboration with Anton Andronic on many topics described in this contribution. This work is supported by the DFG Collaborative Research Centre SFB 1225 (ISOQUANT). PBM thanks Anar Rustamov for important discussions and help with the tex file. K.R. acknowledges the Polish National Science Centre (NCN) support under OPUS Grant No. 2022/45/B/ST2/01527

and of the Polish Ministry of Science and Higher Education. K.R. also acknowledges fruitful discussions with B. Friman, F. Karsch, P.M. Lo and C. Sasaki.

References

1. I. Ya. Pomeranchuk. On the theory of multiple particle production in a single collision. *Dokl. Akad. Nauk SSSR*, 78(5):889–891, 1951.
2. E. Fermi. Multiple Production of Pions in Nucleon-Nucleon Collisions at Cosmotron Energies. *Phys. Rev.*, 92:452–453, 1953.
3. L. D. Landau. On the multiparticle production in high-energy collisions. *Izv. Akad. Nauk Ser. Fiz.*, 17:51–64, 1953.
4. R. Hagedorn. Statistical thermodynamics of strong interactions at high-energies. *Nuovo Cim. Suppl.*, 3:147, 1965.
5. R. Hagedorn. Statistical thermodynamics of strong interactions at high energies. 3. Heavy-pair (quark) production rates. *Nuovo Cim. Suppl.*, 6:311–354, 1968.
6. R. Hagedorn. Hadronic matter near the boiling point. *Nuovo Cim. A*, 56:1027–1057, 1968.
7. J. D. Bjorken and Stanley J. Brodsky. Statistical Model for electron-Positron Annihilation Into Hadrons. *Phys. Rev. D*, 1:1416–1420, 1970.
8. Edward V. Shuryak. Quark-Gluon Plasma and Hadronic Production of Leptons, Photons and Psions. *Phys. Lett. B*, 78:150, 1978.
9. Franz Gross et al. 50 Years of Quantum Chromodynamics. *Eur. Phys. J. C*, 83:1125, 2023.
10. John C. Collins and M. J. Perry. Superdense Matter: Neutrons Or Asymptotically Free Quarks? *Phys. Rev. Lett.*, 34:1353, 1975.
11. N. Cabibbo and G. Parisi. Exponential Hadronic Spectrum and Quark Liberation. *Phys. Lett. B*, 59:67–69, 1975.
12. Edward V. Shuryak. Theory of Hadronic Plasma. *Sov. Phys. JETP*, 47:212–219, 1978.
13. Claudia Ratti and Rene Bellwied. *The Deconfinement Transition of QCD: Theory Meets Experiment*, volume 981 of *Lecture Notes in Physics*. 6 2021.
14. Peter Braun-Munzinger, Krzysztof Redlich, and Johanna Stachel. Particle production in heavy ion collisions. In *Quark Gluon Plasma 3*, eds. R. C. Hwa and Xin-Nian Wang, World Scientific Publishing, 491–599. 2003.
15. Anton Andronic, Peter Braun-Munzinger, Krzysztof Redlich, and Johanna Stachel. Decoding the phase structure of QCD via particle production at high energy. *Nature*, 561(7723):321–330, 2018.
16. Fred Cooper and Graham Frye. Comment on the Single Particle Distribution in the Hydrodynamic and Statistical Thermodynamic Models of Multiparticle Production. *Phys. Rev. D*, 10:186, 1974.
17. Jinhui Chen et al. Properties of the QCD matter: review of selected results from the relativistic heavy ion collider beam energy scan (RHIC BES) program. *Nucl. Sci. Tech.*, 35(12):214, 2024.
18. Misha A. Stephanov, K. Rajagopal, and Edward V. Shuryak. Event-by-event fluctuations in heavy ion collisions and the QCD critical point. *Phys. Rev. D*, 60:114028, 1999.
19. Peter Braun-Munzinger, Volker Koch, Thomas Schäfer, and Johanna Stachel. Properties of hot and dense matter from relativistic heavy ion collisions. *Phys. Rept.*, 621:76–126, 2016.
20. Charles Gale, Sangyong Jeon, and Bjoern Schenke. Hydrodynamic Modeling of Heavy-Ion Collisions. *Int. J. Mod. Phys. A*, 28:1340011, 2013.
21. Raimond Snellings. Elliptic Flow: A Brief Review. *New J. Phys.*, 13:055008, 2011.
22. Jean-Yves Ollitrault, Arthur M. Poskanzer, and Sergei A. Voloshin. Effect of flow fluctuations and nonflow on elliptic flow methods. *Phys. Rev. C*, 80:014904, 2009.
23. R. Baier, Yuri L. Dokshitzer, Alfred H. Mueller, S. Peigne, and D. Schiff. Radiative energy loss and p(T) broadening of high-energy partons in nuclei. *Nucl. Phys. B*, 484:265–282, 1997.

24. Ralf Rapp. Dilepton Spectroscopy of QCD Matter at Collider Energies. *Adv. High Energy Phys.*, 2013:148253, 2013.
25. R. Rapp, J. Wambach, and H. van Hees. The Chiral Restoration Transition of QCD and Low Mass Dileptons. *Landolt-Bornstein*, 23:134, 2010.
26. J. Engels, F. Karsch, H. Satz, and I. Montvay. High Temperature SU(2) Gluon Matter on the Lattice. *Phys. Lett. B*, 101:89, 1981.
27. John B. Kogut, M. Stone, H. W. Wyld, W. R. Gibbs, J. Shigemitsu, Stephen H. Shenker, and D. K. Sinclair. Deconfinement and Chiral Symmetry Restoration at Finite Temperatures in SU(2) and SU(3) Gauge Theories. *Phys. Rev. Lett.*, 50:393, 1983.
28. H. T. Ding et al. Chiral Phase Transition Temperature in (2+1)-Flavor QCD. *Phys. Rev. Lett.*, 123(6):062002, 2019.
29. A. Bazavov et al. Chiral crossover in QCD at zero and non-zero chemical potentials. *Phys. Lett. B*, 795:15–21, 2019.
30. Szabolcs Borsanyi, Zoltan Fodor, Jana N. Guenther, Ruben Kara, Sandor D. Katz, Paolo Parotto, Attila Pasztor, Claudia Ratti, and Kalman K. Szabo. QCD Crossover at Finite Chemical Potential from Lattice Simulations. *Phys. Rev. Lett.*, 125(5):052001, 2020.
31. Gert Aarts et al. Phase Transitions in Particle Physics: Results and Perspectives from Lattice Quantum Chromo-Dynamics. *Prog. Part. Nucl. Phys.*, 133:104070, 2023.
32. Christof Gattringer and Kurt Langfeld. Approaches to the sign problem in lattice field theory. *Int. J. Mod. Phys. A*, 31(22):1643007, 2016.
33. P. Braun-Munzinger, B. Friman, K. Redlich, A. Rustamov, and J. Stachel. Relativistic nuclear collisions: Establishing a non-critical baseline for fluctuation measurements. *Nucl. Phys. A*, 1008:122141, 2021.
34. K. Abe et al. Leading Particle Distributions in 200-GeV/c $P + A$ Interactions. *Phys. Lett. B*, 200:266–271, 1988.
35. J. Benecke, T. T. Chou, Chen-Ning Yang, and E. Yen. Hypothesis of Limiting Fragmentation in High-Energy Collisions. *Phys. Rev.*, 188:2159–2169, 1969.
36. J. D. Bjorken. Highly Relativistic Nucleus-Nucleus Collisions: The Central Rapidity Region. *Phys. Rev. D*, 27:140–151, 1983.
37. Serguei Chatrchyan et al. Measurement of the pseudorapidity and centrality dependence of the transverse energy density in PbPb collisions at $\sqrt{s_{NN}} = 2.76$ TeV. *Phys. Rev. Lett.*, 109:152303, 2012.
38. J. Barrette et al. Measurement of transverse energy production with Si and Au beams at relativistic energy: Towards hot and dense hadronic matter. *Phys. Rev. Lett.*, 70:2996–2999, 1993.
39. M. M. Aggarwal et al. Scaling of particle and transverse energy production in Pb-208 + Pb-208 collisions at 158-A-GeV. *Eur. Phys. J. C*, 18:651–663, 2001.
40. A. Adare et al. Transverse energy production and charged-particle multiplicity at midrapidity in various systems from $\sqrt{s_{NN}} = 7.7$ to 200 GeV. *Phys. Rev. C*, 93(2):024901, 2016.
41. S. Navas et al. Review of particle physics. *Phys. Rev. D*, 110(3):030001, 2024.
42. Andreas Bauswein, Niels-Uwe F. Bastian, David B. Blaschke, Katerina Chatzioannou, James A. Clark, Tobias Fischer, and Micaela Oertel. Identifying a first-order phase transition in neutron star mergers through gravitational waves. *Phys. Rev. Lett.*, 122(6):061102, 2019.
43. Gordon Baym, Shun Furusawa, Tetsuo Hatsuda, Toru Kojo, and Hajime Togashi. New Neutron Star Equation of State with Quark-Hadron Crossover. *Astrophys. J.*, 885:42, 2019.
44. Tyler Gorda, Oleg Komoltsev, and Aleksi Kurkela. Ab-initio QCD Calculations Impact the Inference of the Neutron-star-matter Equation of State. *Astrophys. J.*, 950(2):107, 2023.
45. Johann Rafelski, Jeremiah Birrell, Andrew Steinmetz, and Cheng Tao Yang. A Short Survey of Matter-Antimatter Evolution in the Primordial Universe. *Universe*, 9(7):309, 2023.
46. Roger Dashen, Shang-Keng Ma, and Herbert J. Bernstein. S Matrix formulation of statistical mechanics. *Phys. Rev.*, 187:345–370, 1969.
47. R. Venugopalan and M. Prakash. Thermal properties of interacting hadrons. *Nucl. Phys. A*, 546:718–760, 1992.

48. W. Weinhold, B. Friman, and W. Norenberg. Thermodynamics of Delta resonances. *Phys. Lett. B*, 433:236–242, 1998.
49. Pok Man Lo, Bengt Friman, Krzysztof Redlich, and Chihiro Sasaki. S-matrix analysis of the baryon electric charge correlation. *Phys. Lett. B*, 778:454–458, 2018.
50. Pok Man Lo. Density of states of a coupled-channel system. *Phys. Rev. D*, 102(3):034038, 2020.
51. R. Hagedorn. Thermodynamics of strong interactions. 5 1971.
52. Johann Rafelski. *Melting Hadrons, Boiling Quarks*, pages 417–439. 2016.
53. Kerson Huang and Steven Weinberg. Ultimate temperature and the early universe. *Phys. Rev. Lett.*, 25:895–897, 1970.
54. S. Fubini and G. Veneziano. Level structure of dual-resonance models. *Nuovo Cim. A*, 64:811–840, 1969.
55. H. Satz. Critical Behavior of Hadronic Matter. 1. Critical Point Exponents. *Phys. Rev. D*, 19:1912, 1979.
56. R. Hagedorn and Johann Rafelski. Hot Hadronic Matter and Nuclear Collisions. *Phys. Lett. B*, 97:136, 1980.
57. Pok Man Lo, Michał Marczenko, Krzysztof Redlich, and Chihiro Sasaki. Matching the Hagedorn mass spectrum with Lattice QCD results. *Phys. Rev. C*, 92(5):055206, 2015.
58. Pok Man Lo, Michał Marczenko, Krzysztof Redlich, and Chihiro Sasaki. Missing baryonic resonances in the Hagedorn spectrum. *Eur. Phys. J. A*, 52(8):235, 2016.
59. Wojciech Broniowski and Wojciech Florkowski. Different Hagedorn temperatures for mesons and baryons from experimental mass spectra, compound hadrons, and combinatorial saturation. *Phys. Lett. B*, 490:223–227, 2000.
60. F. Karsch, K. Redlich, and A. Tawfik. Hadron resonance mass spectrum and lattice QCD thermodynamics. *Eur. Phys. J. C*, 29:549–556, 2003.
61. F. Karsch, K. Redlich, and A. Tawfik. Thermodynamics at nonzero baryon number density: A Comparison of lattice and hadron resonance gas model calculations. *Phys. Lett. B*, 571:67–74, 2003.
62. S. Ejiri, F. Karsch, and K. Redlich. Hadronic fluctuations at the QCD phase transition. *Phys. Lett. B*, 633:275–282, 2006.
63. C. R. Allton, M. Doring, S. Ejiri, S. J. Hands, O. Kaczmarek, F. Karsch, E. Laermann, and K. Redlich. Thermodynamics of two flavor QCD to sixth order in quark chemical potential. *Phys. Rev. D*, 71:054508, 2005.
64. A. Bazavov et al. Fluctuations and Correlations of net baryon number, electric charge, and strangeness: A comparison of lattice QCD results with the hadron resonance gas model. *Phys. Rev. D*, 86:034509, 2012.
65. Frithjof Karsch. Thermodynamics of strong interaction matter from lattice QCD and the hadron resonance gas model. *Acta Phys. Polon. Supp.*, 7:117, 2014.
66. A. Bazavov et al. The QCD Equation of State to $O(\mu_B^6)$ from Lattice QCD. *Phys. Rev. D*, 95(5):054504, 2017.
67. Rene Bellwied, Szabolcs Borsanyi, Zoltan Fodor, Jana N. Guenther, Sandor D. Katz, Paolo Parotto, Attila Pasztor, David Pesznyak, Claudia Ratti, and Kalman K. Szabo. Corrections to the hadron resonance gas from lattice QCD and their effect on fluctuation-ratios at finite density. *Phys. Rev. D*, 104(9):094508, 2021.
68. F. Karsch et al. *QCD Phase Structure at Finite Baryon Density*. 2022.
69. Paolo Alba et al. Constraining the hadronic spectrum through QCD thermodynamics on the lattice. *Phys. Rev. D*, 96(3):034517, 2017.
70. D. Bollweg, D. A. Clarke, J. Goswami, O. Kaczmarek, F. Karsch, S. Mukherjee, P. Petreczky, C. Schmidt, and S. Sharma. Equation of state and speed of sound of (2+1)-flavor QCD in strangeness-neutral matter at nonvanishing net baryon-number density. *Phys. Rev. D*, 108(1):014510, 2023.
71. S. Sharma, F. Karsch, and P. Petreczky. Thermodynamics of charmed hadrons across chiral crossover from lattice QCD. *J. Subatomic Part. Cosmol.*, 3:100044, 2025.
72. P. Braun-Munzinger, I. Heppe, and J. Stachel. Chemical equilibration in Pb + Pb collisions at the SPS. *Phys. Lett. B*, 465:15–20, 1999.

73. Anton Andronic, Peter Braun-Munzinger, Bengt Friman, Pok Man Lo, Krzysztof Redlich, and Johanna Stachel. The thermal proton yield anomaly in Pb-Pb collisions at the LHC and its resolution. *Phys. Lett. B*, 792:304–309, 2019.
74. César Fernández-Ramírez, Pok Man Lo, and Peter Petreczky. Thermodynamics of the strange baryon system from a coupled-channels analysis and missing states. *Phys. Rev. C*, 98(4):044910, 2018.
75. Bengt Friman, Pok Man Lo, Michał Marczenko, Krzysztof Redlich, and Chihiro Sasaki. Strangeness fluctuations from $K - \pi$ interactions. *Phys. Rev. D*, 92(7):074003, 2015.
76. K. Redlich and L. Turko. Phase Transitions in the Statistical Bootstrap Model with an Internal Symmetry. *Z. Phys. C*, 5:201, 1980.
77. R. Hagedorn and K. Redlich. Statistical Thermodynamics in Relativistic Particle and Ion Physics: Canonical or Grand Canonical? *Z. Phys. C*, 27:541, 1985.
78. J. Cleymans, K. Redlich, and E. Suhonen. Canonical description of strangeness conservation and particle production. *Z. Phys. C*, 51:137–141, 1991.
79. Jean Cleymans, Helmut Oeschler, and Krzysztof Redlich. Influence of impact parameter on thermal description of relativistic heavy ion collisions at (1-2) A-GeV. *Phys. Rev. C*, 59:1663, 1999.
80. Salah Hamieh, Krzysztof Redlich, and Ahmed Tounsi. Canonical description of strangeness enhancement from p-A to Pb Pb collisions. *Phys. Lett. B*, 486:61–66, 2000.
81. C. M. Ko, V. Koch, Zi-wei Lin, K. Redlich, Misha A. Stephanov, and Xin-Nian Wang. Kinetic equation with exact charge conservation. *Phys. Rev. Lett.*, 86:5438–5441, 2001.
82. Johann Rafelski and Michael Danos. Nuclear matter under extreme conditions. *Lect. Notes Phys.*, 231:361–455, 1985.
83. K. Redlich and A. Tounsi. Strangeness enhancement and energy dependence in heavy ion collisions. *Eur. Phys. J. C*, 24:589–594, 2002.
84. I. Kraus, J. Cleymans, H. Oeschler, and K. Redlich. Particle production in p-p collisions and prediction for LHC energy. *Phys. Rev. C*, 79:014901, 2009.
85. F. Becattini and Ulrich W. Heinz. Thermal hadron production in p p and p anti-p collisions. *Z. Phys. C*, 76:269–286, 1997. [Erratum: Z.Phys.C 76, 578 (1997)].
86. Natasha Sharma, Jean Cleymans, and Lokesh Kumar. Thermal model description of p-Pb collisions at $\sqrt{s_{NN}} = 5.02$ TeV. *Eur. Phys. J. C*, 78(4):288, 2018.
87. A. Andronic, F. Butler, P. Braun-Munzinger, K. Redlich, and J. Stachel. Thermal description of hadron production in e+e- collisions revisited. *Phys. Lett. B*, 675:312–318, 2009.
88. F. Becattini, P. Castorina, J. Manninen, and H. Satz. The Thermal Production of Strange and Non-Strange Hadrons in e+ e- Collisions. *Eur. Phys. J. C*, 56:493–510, 2008.
89. Jaroslav Adam et al. Enhanced production of multi-strange hadrons in high-multiplicity proton-proton collisions. *Nature Phys.*, 13:535–539, 2017.
90. Presented by R. A. Fini et al. Strange baryon production in Pb Pb collisions at 158-A-GeV/c. *J. Phys. G*, 27:375–381, 2001.
91. M. M. Aggarwal et al. Strange and Multi-strange Particle Production in Au+Au Collisions at $\sqrt{s_{NN}} = 62.4$ GeV. *Phys. Rev. C*, 83:024901, 2011. [Erratum: Phys.Rev.C 107, 049903 (2023)].
92. Jean Cleymans, Pok Man Lo, Krzysztof Redlich, and Natasha Sharma. Multiplicity dependence of (multi)strange baryons in the canonical ensemble with phase shift corrections. *Phys. Rev. C*, 103(1):014904, 2021.
93. Vytautas Vislavicius and Alexander Kalweit. Multiplicity dependence of light flavour hadron production at LHC energies in the strangeness canonical suppression picture. 10 2016.
94. J. Cleymans, H. Oeschler, and K. Redlich. Statistical model description of K+ and K- production between 1-GeV/A to 10-GeV/A. *Phys. Lett. B*, 485:27–31, 2000.
95. P. Braun-Munzinger, J. Stachel, and Christof Wetterich. Chemical freezeout and the QCD phase transition temperature. *Phys. Lett. B*, 596:61–69, 2004.
96. L. Adamczyk et al. Bulk Properties of the Medium Produced in Relativistic Heavy-Ion Collisions from the Beam Energy Scan Program. *Phys. Rev. C*, 96(4):044904, 2017.
97. Joachim Stroth, (HADES Collaboration). Private Communications.

98. P. Braun-Munzinger and J. Wambach. The Phase Diagram of Strongly-Interacting Matter. *Rev. Mod. Phys.*, 81:1031–1050, 2009.
99. M. Tanabashi et al. Review of Particle Physics. *Phys. Rev. D*, 98(3):030001, 2018.
100. Steven Weinberg. *The First Three Minutes. A Modern View of the Origin of the Universe*. 1977.
101. Wei-jie Fu, Jan M. Pawłowski, and Fabian Rennecke. QCD phase structure at finite temperature and density. *Phys. Rev. D*, 101(5):054032, 2020.
102. Adam Bzdak, Shinichi Esumi, Volker Koch, Jinfeng Liao, Mikhail Stephanov, and Nu Xu. Mapping the Phases of Quantum Chromodynamics with Beam Energy Scan. *Phys. Rept.*, 853:1–87, 2020.
103. Shreyasi Acharya et al. The ALICE experiment: a journey through QCD. *Eur. Phys. J. C*, 84(8):813, 2024.
104. Anton Andronic, Peter Braun-Munzinger, Markus K. Köhler, Aleksas Mazeliauskas, Krzysztof Redlich, Johanna Stachel, and Vytautas Vislavicius. The multiple-charm hierarchy in the statistical hadronization model. *JHEP*, 07:035, 2021.
105. Anton Andronic, Peter Braun-Munzinger, Markus K. Köhler, Krzysztof Redlich, and Johanna Stachel. Transverse momentum distributions of charmonium states with the statistical hadronization model. *Phys. Lett. B*, 797:134836, 2019.
106. Luis Altenkort, Alexander M. Eller, Olaf Kaczmarek, Lukas Mazur, Guy D. Moore, and Hai-Tao Shu. Heavy quark momentum diffusion from the lattice using gradient flow. *Phys. Rev. D*, 103(1):014511, 2021.
107. Ehab Abbas et al. J/Psi Elliptic Flow in Pb-Pb Collisions at $\sqrt{s_{NN}} = 2.76$ TeV. *Phys. Rev. Lett.*, 111:162301, 2013.
108. Min He, Biaogang Wu, and Ralf Rapp. Collectivity of J/ψ Mesons in Heavy-Ion Collisions. *Phys. Rev. Lett.*, 128(16):162301, 2022.
109. Sungtae Cho, Kai-Jia Sun, Che Ming Ko, Su Houn Lee, and Yongseok Oh. Charmed hadron production in an improved quark coalescence model. *Phys. Rev. C*, 101(2):024909, 2020.
110. Jiaxing Zhao, Shuzhe Shi, Nu Xu, and Pengfei Zhuang. Sequential Coalescence with Charm Conservation in High Energy Nuclear Collisions. 5 2018.
111. Sungtae Cho et al. Exotic hadrons from heavy ion collisions. *Prog. Part. Nucl. Phys.*, 95:279–322, 2017.
112. Kai Zhou, Nu Xu, Zhe Xu, and Pengfei Zhuang. Medium effects on charmonium production at ultrarelativistic energies available at the CERN Large Hadron Collider. *Phys. Rev. C*, 89(5):054911, 2014.
113. V. Greco, C. M. Ko, and R. Rapp. Quark coalescence for charmed mesons in ultrarelativistic heavy ion collisions. *Phys. Lett. B*, 595:202–208, 2004.
114. G. Aarts et al. Heavy-flavor production and medium properties in high-energy nuclear collisions - What next? *Eur. Phys. J. A*, 53(5):93, 2017.
115. Luciano Maiani and Alessandro Pilloni. GGI Lectures on Exotic Hadrons. 7 2022.
116. Taesoo Song and Gabriele Coci. Prerequisites for heavy quark coalescence in heavy-ion collisions. 4 2021.
117. Shreyasi Acharya et al. Measurement of inclusive J/ψ production at midrapidity and forward rapidity in Pb-Pb collisions at $\sqrt{s_{NN}} = 5.02$ TeV. 2022.
118. P. Braun-Munzinger and J. Stachel. (Non)thermal aspects of charmonium production and a new look at J/ψ suppression. *Phys. Lett. B*, 490:196–202, 2000.
119. A. Andronic, P. Braun-Munzinger, K. Redlich, and J. Stachel. Statistical hadronization of charm at SPS, RHIC and LHC. *Nucl. Phys. A*, 715:529–532, 2003.
120. Loic Grandchamp, Ralf Rapp, and Gerald E. Brown. In medium effects on charmonium production in heavy ion collisions. *Phys. Rev. Lett.*, 92:212301, 2004.
121. Francesco Becattini. Production of multiply heavy flavored baryons from quark gluon plasma in relativistic heavy ion collisions. *Phys. Rev. Lett.*, 95:022301, 2005.
122. A. Andronic, P. Braun-Munzinger, K. Redlich, and J. Stachel. Statistical hadronization of heavy quarks in ultra-relativistic nucleus-nucleus collisions. *Nucl. Phys. A*, 789:334–356, 2007.

123. Peter Braun-Munzinger, Krzysztof Redlich, Natasha Sharma, and Johanna Stachel. Emergence of new systematics for open charm production in high energy collisions. *JHEP*, 04:058, 2025.
124. T. Matsui and H. Satz. J/ψ Suppression by Quark-Gluon Plasma Formation. *Phys. Lett. B*, 178:416–422, 1986.
125. Letter of intent for ALICE 3: A next-generation heavy-ion experiment at the LHC. 11 2022.
126. Shreyasi Acharya et al. Measurements of Chemical Potentials in Pb-Pb Collisions at $s_{\text{NN}}=5.02$ TeV. *Phys. Rev. Lett.*, 133(9):092301, 2024.
127. A. Bazavov et al. The melting and abundance of open charm hadrons. *Phys. Lett. B*, 737:210–215, 2014.
128. A. Bazavov, D. Bollweg, O. Kaczmarek, F. Karsch, Swagato Mukherjee, P. Petreczky, C. Schmidt, and S. Sharma. Charm degrees of freedom in hot matter from lattice QCD. *Phys. Lett. B*, 850:138520, 2024.
129. Kai Zhou, Zhengyu Chen, Carsten Greiner, and Pengfei Zhuang. Thermal Charm and Charmonium Production in Quark Gluon Plasma. *Phys. Lett. B*, 758:434–439, 2016.
130. A. Dainese et al. Heavy ions at the Future Circular Collider. 5 2016.
131. A. Andronic, P. Braun-Munzinger, and J. Stachel. Hadron production in central nucleus-nucleus collisions at chemical freeze-out. *Nucl. Phys. A*, 772:167–199, 2006.
132. J. Cleymans, H. Oeschler, K. Redlich, and S. Wheaton. Comparison of chemical freeze-out criteria in heavy-ion collisions. *Phys. Rev. C*, 73:034905, 2006.
133. Anton Andronic, Peter Braun-Munzinger, Hjalmar Brunßen, Jana Crkovská, Johanna Stachel, Vytautas Vislavicius, and Martin Völkl. Transverse dynamics of charmed hadrons in ultra-relativistic nuclear collisions. *JHEP*, 10:229, 2024.
134. Francesco Becattini. A Thermodynamical approach to hadron production in e+ e- collisions. *Z. Phys. C*, 69(3):485–492, 1996.